Ann. Rev. Phys. Chem. 1982. 33:119–50

PHOTOFRAGMENT ALIGNMENT AND ORIENTATION

Chris H. Greene

Department of Physics and Astronomy, Louisiana State University, Baton Rouge, Louisiana 70803

Richard N. Zare

Department of Chemistry, Stanford University, Stanford, California 94305

INTRODUCTION

Early measurements demonstrated long ago the wealth of chemical information that can be extracted from photofragmentation experiments in which a target system is dissociated or ionized following the absorption of a sufficiently energetic photon (1–8). For many years experimentalists measured primarily *total* photofragmentation cross sections or rate constants. More recently, a relatively few studies have determined some measure of the *anisotropy* characterizing the photofragmentation process (9–20). In contrast to isotropic rate constant measurements that ignore all directional information, measurements of fragment anisotropy give a much more detailed picture of the dynamics of the photoejection process. In the past it has been common to consider separately photodissociation of isolated molecules and photoionization of free atoms or molecules. In what follows we shall call photodissociation/photoionization by the single name, *photofragmentation*, for, as we show, both processes can be treated together in a unified manner.

0066-426X/82/1101-0119$02.00

The anisotropy receiving most attention to date has been the photofragment angular distribution. For photofragmentation by a beam of linearly polarized light this distribution takes the form

$$\frac{d\sigma}{d\Omega} = \frac{\sigma}{4\pi}\left[1+\beta P_2(\cos\theta)\right] \qquad 1.$$

for an electric dipole transition, where θ is the angle between the final recoil direction of the fragments and the electric vector of the light beam. Note that Eq. 1 applies to a single-photon process whereby the target breaks up into only two fragments. Measurements of the anisotropy parameter β in photoionization experiments (6–8, 21–33) have been instrumental in testing various theories of electron correlation (20, 34–37) and have helped unravel the complicated couplings of electronic, vibrational, and rotational motions in molecules (38–45). Measurements of β in photodissociation experiments have yielded information on the symmetry nature of the dissociative molecular state and the time required for the fragments to escape from the excited complex (10–14, 46).

In this article we consider primarily another anisotropy, namely the alignment or orientation of individual fragments. Angular momentum is transferred from the light beam to the ensemble of fragments. Not only does each fragment quantum state have a given energy E but also a definite angular momentum $\mathbf{J}$ defined in magnitude and quantized in space. To make the concepts of alignment and orientation concrete, let us consider the case of an ensemble of fragments with total angular momentum $J=2$. If we need to account only for the occupation probabilities of the five magnetic sublevels, $M=2,1,0,-1,-2$, then the five-dimensional vector

$$\mathbf{N} = \begin{vmatrix} N_2 \\ N_1 \\ N_0 \\ N_{-1} \\ N_{-2} \end{vmatrix} \qquad 2.$$

suffices, where N_M is the number of fragments in the state $|JM\rangle$.

Note: Equation 2 assumes that the system has cylindrical symmetry. More generally, the excited state ensemble must be represented by a $(2J+1)\times(2J+1)$ density matrix $\boldsymbol{\rho}$ whose diagonal elements $\rho_{MM} = \langle JM|\boldsymbol{\rho}|JM\rangle$ represent occupation numbers (populations) in the levels M and whose off-diagonal elements $\rho_{M'M} = \langle JM'|\boldsymbol{\rho}|JM\rangle$ represent coherence terms (containing phase information) between the M' and M

levels. It is useful to introduce the spherical tensor operators (47–50)

$$T(J)_{LM_L} = \sum_{M,M'} (-1)^{J-M} (JM', J-M \mid LM_L) \mid JM' \rangle \langle JM \mid$$

which satisfy the orthonormality conditions

$$Tr\left[T(J)^{\dagger}_{LM_L} T(J)_{L'M'_L}\right] = \mathbf{T}(J)^{*}_{LM_L} \cdot \mathbf{T}(J)_{L'M'_L} = \delta_{LL'} \delta_{M_L M'_L}$$

and behave under rotation like the spherical harmonics Y_{LM_L}. The restriction on the Clebsch-Gordan coefficient $(JM', J-M \mid LM_L)$ shows that L ranges from 0 to $2J$ and M_L ranges in unit steps from $-L$ to L. Hence the $\mathbf{T}(J)_{LM_L}$ span the $(2J+1)\times(2J+1)$ space of the density matrix. Specifically, we may decompose $\boldsymbol{\rho}$ as

$$\boldsymbol{\rho} = \sum_{L,M_L} \rho_{LM_L} \mathbf{T}_{LM_L}$$

where the expansion coefficients ρ_{LM_L}, given by

$$\rho_{LM_L} = Tr\left[\mathbf{T}^{\dagger}_{LM_L} \boldsymbol{\rho}\right] = \mathbf{T}^{*}_{LM_L} \cdot \boldsymbol{\rho} = \langle T^{\dagger}_{LM_L} \rangle Tr[\boldsymbol{\rho}],$$

are the multipole moments of the system. When $M_L = 0$ we recover the $\hat{\mathbf{T}}_L \equiv \langle T^{\dagger}_{LO}(J) \rangle$ whose $2J+1$ elements of the form $(-1)^{J-M}(JM, J-M \mid LO)$ are the same as displayed in Eq. 4 for the case of a $J=2$ system.

This vector can of course be expanded as a linear combination of the "Cartesian" basis vectors:

$$\begin{pmatrix} 1 \\ 0 \\ 0 \\ 0 \\ 0 \end{pmatrix}, \quad \begin{pmatrix} 0 \\ 1 \\ 0 \\ 0 \\ 0 \end{pmatrix}, \quad \begin{pmatrix} 0 \\ 0 \\ 1 \\ 0 \\ 0 \end{pmatrix}, \quad \begin{pmatrix} 0 \\ 0 \\ 0 \\ 1 \\ 0 \end{pmatrix}, \quad \begin{pmatrix} 0 \\ 0 \\ 0 \\ 0 \\ 1 \end{pmatrix}. \qquad 3.$$

However, to bring out the symmetries of the system it is much more convenient to introduce the "spherical" basis vectors:

$$\hat{\mathbf{T}}_0 = \frac{1}{\sqrt{5}} \begin{pmatrix} 1 \\ 1 \\ 1 \\ 1 \\ 1 \end{pmatrix}, \quad \hat{\mathbf{T}}_1 = \frac{1}{\sqrt{10}} \begin{pmatrix} 2 \\ 1 \\ 0 \\ -1 \\ -2 \end{pmatrix}, \quad \hat{\mathbf{T}}_2 = \frac{1}{\sqrt{14}} \begin{pmatrix} 2 \\ -1 \\ -2 \\ -1 \\ 2 \end{pmatrix},$$

$$\hat{\mathbf{T}}_3 = \frac{1}{\sqrt{10}} \begin{pmatrix} 1 \\ -2 \\ 0 \\ 2 \\ -1 \end{pmatrix}, \quad \hat{\mathbf{T}}_4 = \frac{1}{\sqrt{70}} \begin{pmatrix} 1 \\ -4 \\ 6 \\ -4 \\ 1 \end{pmatrix}, \qquad 4.$$

which satisfy the orthonormality condition

$$\hat{\mathbf{T}}_i \cdot \hat{\mathbf{T}}_j = \delta_{ij}. \qquad 5.$$

Then $\mathbf{N}$ may be expanded in terms of the $\hat{\mathbf{T}}_L$ basis set as

$$\mathbf{N} = \sum_{L=0}^{4} n_L \hat{\mathbf{T}}_L \qquad 6.$$

where the coefficients $n_L = \hat{\mathbf{T}}_L \cdot \mathbf{N}$ represent the 2^L multipole moments of $\mathbf{N}$.

For $L = 0$

$$n_0 = \frac{1}{\sqrt{5}} (N_2 + N_1 + N_0 + N_{-1} + N_{-2}) \qquad 7.$$

is proportional to the total number of $J = 2$ fragments. It is called the monopole component of $\mathbf{N}$. For $L = 1$

$$n_1 = \frac{1}{\sqrt{10}} (2N_2 + N_1 - N_{-1} - 2N_{-2})$$

$$= \frac{1}{\sqrt{2}} n_0 \langle J_z \rangle \qquad 8.$$

is proportional to the magnetic dipole moment of the ensemble and is known as the *orientation*. For $L = 2$

$$n_2 = \frac{1}{\sqrt{14}} (2N_2 - N_1 - 2N_0 - N_{-1} + 2N_{-2})$$

$$= \frac{1}{3} \sqrt{\frac{5}{14}}\, n_0 \langle 3J_z^2 - \mathbf{J}^2 \rangle \qquad 9.$$

is proportional to the quadrupole moment of $\mathbf{N}$ and is known as the *alignment*. Similarly

$$n_3 = \frac{1}{\sqrt{10}} (N_2 - 2N_1 + 2N_{-1} - N_{-2})$$

$$= \frac{1}{6\sqrt{2}} n_0 \langle J_z (5J_z^2 + 1 - 3\mathbf{J}^2) \rangle \qquad 10.$$

and

$$n_4 = \frac{1}{\sqrt{70}} (N_2 - 4N_1 + 6N_0 - 4N_{-1} + N_{-2})$$

$$= \frac{1}{12\sqrt{14}} n_0 \langle 3\mathbf{J}^2 [\mathbf{J}^2 - 2(5J_z^2 + 1)] + 5J_z^2 (7J_z^2 + 5) \rangle \qquad 11.$$

are the octopole and hexadecapole moments of $\mathbf{N}$, respectively. The M state population is completely described by the n_L coefficients. For arbitrary (integral or half-integral) J there are in general $2J+1$ different multipole moments. As J becomes large we approach the classical correspondence limit and the n_L become the average value of the Legendre polynomials $\langle P_L(\hat{\mathbf{J}}\cdot\hat{\mathbf{z}})\rangle$, i.e. the classical multipole moments of the angular momentum distribution. Indeed the orientation and the alignment are strictly proportional to

$$\langle P_1(\hat{\mathbf{J}}\cdot\hat{\mathbf{z}})\rangle = \langle J_z\rangle/|\mathbf{J}| \quad \text{and} \quad \langle P_2(\hat{\mathbf{J}}\cdot\hat{\mathbf{z}})\rangle = \langle \tfrac{1}{2}(3J_z^2-\mathbf{J}^2)/\mathbf{J}^2\rangle,$$

respectively, for all J. However, this identification of n_L with $\langle P_L(\hat{\mathbf{J}}\cdot\hat{\mathbf{z}})\rangle$ only holds for $L \geqslant 3$ in the high J classical limit.

Figure 1 illustrates the form of these distributions for a $J=2$ system. If the only moment present is that of the monopole, then all the magnetic

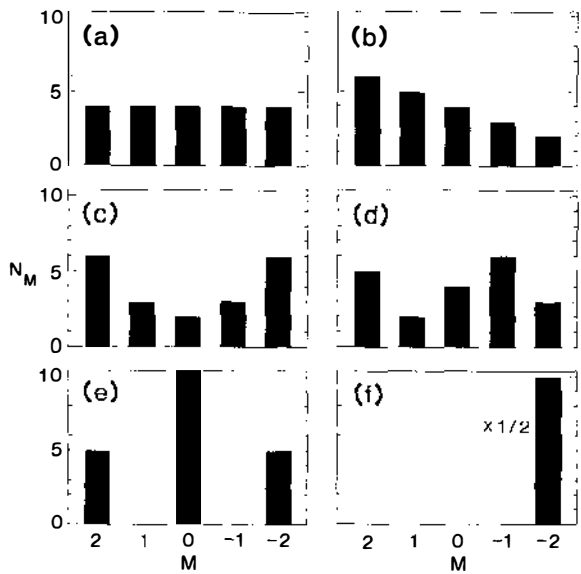

Figure 1 Population versus M state for a $J=2$ system showing the distribution for (*a*) a pure monopole moment, $\mathbf{N}=4\sqrt{5}\,\hat{\mathbf{T}}_0$, (*b*) a monopole plus dipole moment, $\mathbf{N}=4\sqrt{5}\,\hat{\mathbf{T}}_0+\sqrt{10}\,\hat{\mathbf{T}}_1$, (*c*) a monopole plus quadrupole moment, $\mathbf{N}=4\sqrt{5}\,\hat{\mathbf{T}}_0+\sqrt{14}\,\hat{\mathbf{T}}_2$, (*d*) a monopole plus octopole moment, $\mathbf{N}=4\sqrt{5}\,\hat{\mathbf{T}}_0+\sqrt{10}\,\hat{\mathbf{T}}_3$, (*e*) a monopole plus hexadecapole moment, $\mathbf{N}=4\sqrt{5}\,\hat{\mathbf{T}}_0+\sqrt{70}\,\hat{\mathbf{T}}_4$, and (*f*) a special mixed state in which all the population is in the $M=-2$ sublevel. The latter may be decomposed into a linear superposition of multipole moments, specifically, $\mathbf{N}=4\sqrt{5}\,\hat{\mathbf{T}}_0-4\sqrt{10}\,\hat{\mathbf{T}}_1+20\sqrt{2/7}\,\hat{\mathbf{T}}_2-2\sqrt{10}\,\hat{\mathbf{T}}_3+2\sqrt{10/7}\,\hat{\mathbf{T}}_4$. It is natural to define the polarization of the system as the difference between the actual multipole moment distribution and the distribution of an unpolarized ensemble, corresponding to equal occupation of all the magnetic sublevels [shown in (*a*)]. Thus (*b*) describes pure orientation while (*c*) describes pure alignment.

sublevels are equally populated. We also see that for orientation (and other odd multipoles) the population of $+M$ and $-M$ sublevels differ while for alignment (and other even multipoles) the population may be unequal only for different $|M|$ values.

Experimentally, the orientation or alignment of an excited state fragment is most easily determined by measuring the polarization of its fluorescence (14, 51, 52). The orientation or alignment of a ground state fragment (as well as the octopole and hexadecapole moments) can alternatively be extracted using laser-induced fluorescence (53), but we do not discuss this topic here. To date, only a handful of such emission polarization measurements have been carried out, with the result that fragment polarization is observed in almost every case (54–72). The mere observation of nonzero polarization is not surprising of course, since the incident photon is itself highly anisotropic and the subsequent fragmentation is such a violent event. Now that this polarization has been demonstrated, we can begin to use such measurements as a comprehensive tool for learning about the dynamics of the photofragmentation process and the resulting fragment charge distributions. The remainder of this article addresses the problem of extracting useful dynamical information from polarization measurements.

This is far from the first study of this problem. Starting in the 1950s, the physico-mathematical methods required were developed within the context of perturbed angular correlations of nuclei (48, 73–76). Using density matrix techniques and the powerful methods of Racah algebra, the polarization of light emitted from a fragment was related to the multipole moments of the fragment excited state. This approach derived essentially all the relevant formulae necessary to invert a measurement of polarized emission (or resonance fluorescence) and determine the desired fragment multipole moments. But owing to the heavy use of angular momentum coupling machinery, these results have not been immediately accessible to most experimentalists interested in probing molecular dynamics. Significant progress toward dispelling this obscurity was achieved in the 1973 review article of Fano & Macek (FM) (77). That article obtains the general expression for the intensity I of polarized light emitted in any direction following an arbitrary excitation process, expressing I in terms of simple *geometrical* factors and a few *dynamical* parameters describing the excited fragment multipole moments. Fano & Macek thus provided a unified framework for disentangling dynamical from geometrical information based on emission polarization measurements performed after some type of "collisional" excitation. Here the collision refers to excitation by bombardment with photons, electrons, or even heavy particles. A first goal for the present article is to summarize

the main results of FM, both because we hope to broaden its application in the chemical domain, and because the FM framework provides a convenient basis for expressing the results of what follows.

The second goal of this article is to present an interpretation of the measured orientation or alignment, indicating what the fragment multipole moments imply about the photofragmentation process. At the heart of this treatment is the angular momentum transfer formulation of Fano & Dill (78–80). This formulation demonstrates how only three dynamical amplitudes, or more precisely, their two mutual ratios, determine the orientation or alignment of a photofragment, in contrast to the (often) enormous number of continuum amplitudes that enter the more usual formulations of photofragmentation scattering dynamics. This treatment is carried out for arbitrary angular momentum but special attention is given to the high J limit characteristic of many molecular processes.

THE FANO-MACEK FORMULATION OF ORIENTATION AND ALIGNMENT

We begin by considering in Figure 2 the simplest and most common experimental geometry in which a photon beam $h\nu$ impinges on a gas of randomly oriented target molecules or atoms. After absorbing a photon, the target species dissociates or ionizes, leaving, for example, a fragment A (atom or molecule) in an excited state with angular momentum $\mathbf{J}_i$. At 90° with respect to the photon symmetry axis $\hat{\mathbf{z}}$, a fluorescence photon (emitted in the transition $J_i \rightarrow J_f$) is detected using a linear polarizer set at an angle χ relative to the z axis. Two experimental quantities are usually of interest:

1. The total intensity I_0 of light with energy $h\nu'$ emitted in all directions, which is proportional to the population (monopole moment n_0) of the excited state $\mathbf{J}_i$.
2. The linear polarization of this light, defined as $P = (I_{\parallel} - I_{\perp})/(I_{\parallel} + I_{\perp})$, with $I_{\parallel}$ and $I_{\perp}$ the intensities observed when the linear polarizer is set at $\chi = 0$ and $\chi = 90°$, respectively, which is a measure of the alignment (quadrupole moment n_2) of the excited state $\mathbf{J}_i$.

Here the total intensity I_0 is most usually of interest when the partial cross section for creating fragments $A(J_i)$ is desired. One obvious, but impractical, way of measuring I_0 is to detect all photons emitted into all directions with arbitrary polarizations. This measurement is independent of the collision-produced anisotropy. On the other hand, if the more usual experimental geometry of Figure 2 is adopted, care must be

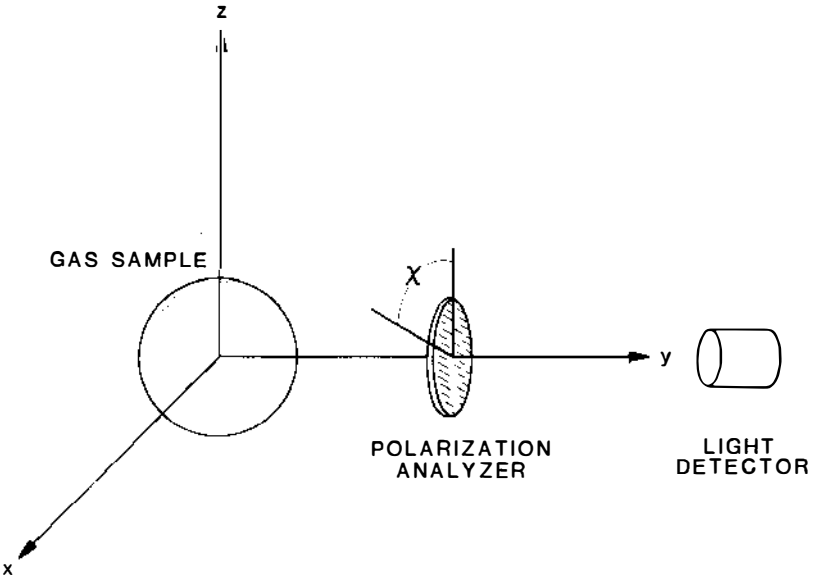

Figure 2 Traditional right-angle geometry for measuring emission polarization. The z axis is the photon symmetry axis directed along the electric vector for a plane polarized light beam or along the propagation direction for an unpolarized light beam. The polarization-analyzer light-detector combination lies in the xy plane and its direction is taken to define the y axis. The transmission axis of the linear polarizer makes the angle χ with respect to the z axis such that the setting $\chi = 0$ corresponds to the transmission of the $I_{\parallel}$ light signal and $\chi = 90°$ to $I_{\perp}$.

exercised since the intensity of polarized or even of unpolarized light depends on the alignment and is thus not proportional to I_0 alone. The second experimental quantity of interest, P, depends directly on the alignment and vanishes if there is no alignment. Yet the measurement of P with the experimental setup of Figure 2 may prove difficult, for example, if the fluorescent photons lie in the vacuum ultraviolet spectrum where suitable polarizing materials are not readily available. One major motivation for presenting the general formulation of light emission here is to show the possibility of alternative experimental methods of obtaining the same information about the atomic or molecular system.

Excitation-Detection Geometry

The right-angle setup of Figure 2 is a specialized case of the more general arrangement shown in Figure 3, where there are two coordinate frames of interest. The first, or "collision frame" of coordinates (x,y,z), is adapted to the symmetry of the exciting collision, with the z axis chosen to be its dominant symmetry axis. When no other axis is singled out by the

collision, the collision frame is cylindrically symmetric and the choice of the x and y coordinates is arbitrary. For example, in a molecular photodissociation experiment using unpolarized incident photons,

$$h\nu + \mathrm{AB} \rightarrow \mathrm{A}^*(J_i) + \mathrm{B}$$
$$\hookrightarrow \mathrm{A}(J_f) + h\nu'$$

the incident photon beam axis serves as the z axis. But if B is detected along a new axis $\hat{\mathbf{w}}$ in coincidence with the fluorescence photon, the cylindrical symmetry is destroyed. For this more complicated coincidence experiment, a plane of symmetry still exists, namely the wz plane. By

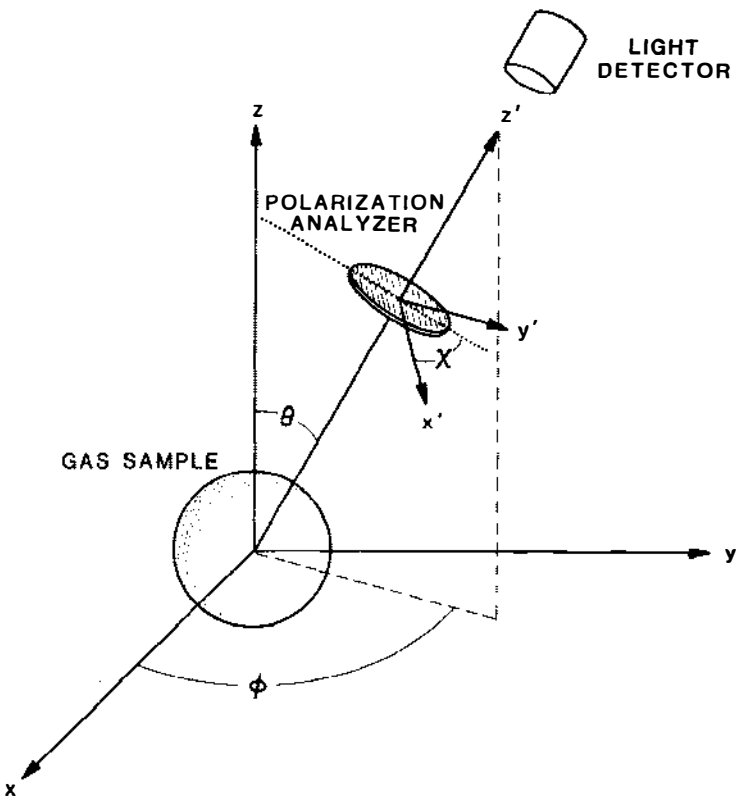

Figure 3 The collision frame x, y, z and the detector frame x′, y′, z′ defining the Euler angles ϕ, θ, χ. The angles θ and ϕ are the polar angles of the axis of the light detector (the z′ axis) referred to the collision frame. The angle χ is measured between the transmission axis of the polarization analyzer (the x′ axis) and the zz′ plane, i.e. between the x′ axis and a line drawn normal to the detector axis which intersects the z axis.

convention the x and y coordinates of the collision frame in this problem are chosen so that $\hat{\mathbf{y}}$ is parallel to $\hat{\mathbf{z}}\times\hat{\mathbf{w}}$.

Although the physics of the collision is described most naturally in the collision frame, the detection of the fluorescence photon is better described in a "detector frame" of coordinates (x′,y′,z′). The direction of observation of the photon is taken as the z′ axis, so its polarization vector $\hat{\mathcal{E}}$ is confined to the x′y′ plane. In the detector frame the detected polarization vector $\hat{\mathcal{E}}$ can be written

$$\hat{\mathcal{E}} = (\cos\beta, i\sin\beta, 0) \qquad 12.$$

Thus $\beta = 0$ represents the observation of light which is linearly polarized along x′, while $\beta = \pi/4$ represents the detection of left-circularly polarized light (81). The multipole moments in the two coordinate frames are related using rotation matrices, whose arguments (ϕ, θ, χ) are the Euler angles required to rotate (x,y,z) into (x′,y′,z′), as shown in Figure 3.

Source Anisotropy and the Emitted Light

We present and discuss the results of Fano & Macek that relate the excited state fragment multipole moments to the distribution of its emitted light. For details regarding derivations, their original article should be consulted. The first key result is the intensity of fluorescence from the transition $J_i \to J_f$ which is observed by a light detector sensitive to the polarization characterized by β as in Eq. 12:

$$I = \tfrac{1}{3}I_0\Big\{1 - \tfrac{1}{2}h^{(2)}(J_i, J_f)\mathcal{Q}_0^{\det} + \tfrac{3}{2}h^{(2)}(J_i, J_f)\mathcal{Q}_{2+}^{\det}\cos 2\beta + \tfrac{3}{2}h^{(1)}(J_i, J_f)\mathcal{O}_0^{\det}\sin 2\beta\Big\}. \qquad 13.$$

Here the light intensity detected at a particular location is expressed in terms of two new kinds of quantities. First, the $h^{(k)}(J_i, J_f)$ ($k = 1$ or 2) are functions that depend only on the angular momentum quantum numbers of the initial (J_i) and final (J_f) fragment states. Thus the $h^{(k)}(J_i, J_f)$ are *geometrical* quantities which are independent of the fragmentation dynamics. Second, the quantities $\mathcal{Q}_0^{\det}, \mathcal{Q}_{2+}^{\det}, \mathcal{O}_0^{\det}$ are the expectation values of multipole moment operators of the fragment excited state, which thus contain all the *dynamical* information about the excited state that can be learned from a fluorescence measurement. More explicitly, these multipole moments are the expectation values of certain combinations of angular momentum operators in the "primed" detector frame of Figure 3:

$$\begin{aligned}
\mathcal{Q}_0^{\det} &= \langle (J_i | 3J_{z'}^2 - \mathbf{J}^2 | J_i) \rangle / J_i(J_i+1), \\
\mathcal{Q}_{2+}^{\det} &= \langle (J_i | J_{x'}^2 - J_{y'}^2 | J_i) \rangle / J_i(J_i+1), \\
\mathcal{O}_0^{\det} &= \langle (J_i | J_{z'} | J_i) \rangle / \sqrt{J_i(J_i+1)}.
\end{aligned} \qquad 14.$$

The expectation values of operators in Eq. 14 require some explanation. The matrix element $\langle (J_i | J_{z'} | J_i) \rangle$, for example, is an average over several excited state matrix elements of the usual type found in quantum mechanics $(J_i M_i | J_{z'} | J_i M_i')$, but weighted according to the distribution of M_i quantum numbers populated in the excited fragment state. In explicit density matrix language (50, 82), we say that a collision creates an excited state density matrix $\rho_{M_i' M_i}$. Then the brackets $\langle\ \rangle$ in Eq. 14 imply the usual trace operation:

$$\langle (J_i | J_{z'} | J_i) \rangle = \sum_{M_i, M_i'} \rho_{M_i' M_i} (J_i M_i | J_{z'} | J_i M_i'). \qquad 15.$$

From an experimental or operational point of view it is not necessary to introduce density matrices, but in the language of density matrices the measurement of orientation or alignment corresponds to the measurement of the first and second rank multipole moments of the density matrix.

Comparison of Eq. 12 and Eq. 13 shows how the term $1 - \frac{1}{2} h^{(2)}(J_i, J_f) \mathcal{A}_0^{\text{det}}$ is observed by an unpolarized detector $(I_\parallel + I_\perp)$, proportional to the sum of $\beta = 0$ and $\pi/2$, the term $\frac{3}{2} h^{(2)}(J_i, J_f) \mathcal{A}_{2+}^{\text{det}} \cos 2\beta$ is observed when linear polarization $(I_\parallel - I_\perp)$ is detected, proportional to the difference of $\beta = 0$ and $\pi/2$, and finally the term $\frac{3}{2} h^{(1)}(J_i, J_f) \mathcal{O}_0^{\text{det}} \sin 2\beta$ is observed only through a circular polarizer, $\beta = \pm \pi/4$. Thus $\mathcal{A}_0^{\text{det}}$ and $\mathcal{A}_{2+}^{\text{det}}$ are two irreducible elements of the quadrupole-moment matrix (of rank $k = 2$) of the excited state, while $\mathcal{O}_0^{\text{det}}$ is the z′-component of an excited state magnetic dipole moment (rank $k = 1$).

The functions $h^{(k)}(J_i, J_f)$ are important in that they isolate the sole effect of the final state $|J_f)$ on the distribution of emitted polarized light. They reflect the amount of information lost when light is emitted and no further observations are made on the final state. Derived by Fano & Macek (77) as a ratio of Wigner $6j$ coefficients, they are given explicitly in Table 1. The definitions of the alignment tensor $\mathcal{A}^{\text{det}}$ and depolarization coefficient $h^{(2)}(J_i, J_f)$ given here coincide with those of Fano & Macek (77). We have found it convenient to modify their definitions of $\mathcal{O}^{\text{det}}$ and $h^{(1)}(J_i, J_f)$, however. Our orientation vector $\mathcal{O}^{\text{det}}$ is $\sqrt{J_i(J_i+1)}$ times that of FM, while the coefficient $h^{(1)}(J_i, J_f)$ is $1/\sqrt{J_i(J_i+1)}$ times that of FM, which ensures that both $\mathcal{O}^{\text{det}}$ and $h^{(1)}(J_i, J_f)$ remain finite in the limit $J_i \to \infty$.

In writing the anisotropy tensor elements $(\mathcal{A}_0^{\text{det}}, \mathcal{A}_{2+}^{\text{det}}, \mathcal{O}_0^{\text{det}})$ in a "detector"-based coordinate system (x′, y′, z′), we have not utilized the known symmetry of the exciting collision, which is clearly better described in the "collision" frame (x, y, z) of Figure 3. Although only three multipole elements in the detector frame are relevant to light emission, there may be more moments in the collision frame or possibly less, depending on

Table 1 The geometrical factors $h^{(k)}(J_i, J_f)$ for the $J_i \to J_f$ transition

J_f	Emission branch	$h^{(1)}(J_i, J_f)$	$h^{(2)}(J_i, J_f)$
J_i+1	$P\downarrow$	$\frac{J_i}{\sqrt{J_i(J_i+1)}}$	$\frac{J_i}{2J_i+3}$
J_i	$Q\downarrow$	$\frac{1}{\sqrt{J_i(J_i+1)}}$	1
J_i-1	$R\downarrow$	$\frac{J_i+1}{\sqrt{J_i(J_i+1)}}$	$-\frac{J_i+1}{2J_i-1}$

the symmetry of the collision process. Rather than introducing the tensorial considerations required to formulate this problem in complete generality, we proceed to treat the most common and simplest symmetry case first.

Cylindrically Symmetric Collision Frame

Collisions like the one depicted in Figure 2, in which only one axis $\hat{\mathbf{z}}$ is singled out, have cylindrical symmetry about that axis. Consequently only axially symmetric tensor elements $T_q^{(k)}$ with $q=0$ can be nonzero in this frame. For the present problem the collision frame alignment tensor $\mathcal{A}$ has only the element $\mathcal{A}_0$ (denoted $\mathcal{A}_0^{\text{col}}$ in FM) and the orientation vector $\mathcal{O}$ has only a nonzero z-component $\mathcal{O}_0$ (denoted $\mathcal{O}_0^{\text{col}}$ in FM). Moreover $\mathcal{O}$ is the mean value of a *pseudovector* **J**, and must accordingly vanish unless any of the collision partners have an initial net orientation or helicity themselves. For the experiment of Figure 2, where the target molecules AB are randomly oriented, we then have three possibilities:

1. The incident photons are unpolarized and incident along $\hat{\mathbf{z}}$. Then $\mathcal{O}$ vanishes identically and $\mathcal{A}_0$ is the only nonzero anisotropy in the collision frame.
2. The incident photons are linearly polarized along $\hat{\mathbf{z}}$. Here also $\mathcal{O}$ vanishes and $\mathcal{A}_0$ is the only nonzero anisotropy. The measured value of $\mathcal{A}_0$ for linearly polarized photons is equal to -2 multiplied by the value of $\mathcal{A}_0$ obtained with unpolarized photons.
3. The incident photons are circularly polarized along the incidence axis $\hat{\mathbf{z}}$. Now both $\mathcal{A}_0$ and $\mathcal{O}_0$ are nonzero. The alignment $\mathcal{A}_0$ obtained with circularly polarized light is the same as that obtained with unpolarized light. Note that the values of $\mathcal{O}_0$ obtained with right- and

with left-circularly polarized light have the same magnitude but opposite signs.

The results 1–3 do not rely on the fact that we are discussing photodissociation. They apply equally to any photofragmentation experiment in which the target molecules or atoms are randomly aligned and oriented.

To utilize the collision frame symmetries of $\mathcal{A}$ and $\mathcal{O}$ we must relate them to the detector frame quantities $\mathcal{A}^{\text{det}}$ and $\mathcal{O}^{\text{det}}$ which determine the light distribution through Eq. 13. This relationship is obtained by FM using rotation matrices.[1] In terms of the Euler angles (ϕ, θ, χ) defined in Figure 3, FM obtain for a cylindrically symmetric collision frame the results:

$$\mathcal{A}_0^{\text{det}} = \mathcal{A}_0 P_2(\cos\theta), \quad \mathcal{A}_{2+}^{\text{det}} = \mathcal{A}_0\left(\tfrac{1}{2}\sin^2\theta\cos 2\chi\right),$$
$$\mathcal{O}_0^{\text{det}} = \mathcal{O}_0\cos\theta, \qquad 16.$$

where $P_2(\cos\theta) = \frac{3}{2}\cos^2\theta - \frac{1}{2}$ is the second rank Legendre polynomial, and where $\mathcal{A}_0$ and $\mathcal{O}_0$ are given by Eq. 14 with the primes removed. Inserting these into Eq. 13 gives the distribution of light emitted as a function of the polar coordinates (θ, ϕ) of the light detector and the orientation χ of its polarization analyzer for a collision frame having cylindrical symmetry. The result is

$$\begin{aligned} I(\phi, \theta, \chi) = \tfrac{1}{3}I_0\Big\{ & 1 - \tfrac{1}{2}h^{(2)}(J_i, J_f)\mathcal{A}_0 P_2(\cos\theta) \\ & + \tfrac{3}{4}h^{(2)}(J_i, J_f)\mathcal{A}_0\sin^2\theta\cos 2\chi\cos 2\beta \\ & + \tfrac{3}{2}h^{(1)}(J_i, J_f)\mathcal{O}_0\cos\theta\sin 2\beta\Big\}. \qquad 17. \end{aligned}$$

In the most common experiments, using either linearly polarized or unpolarized incident light, $\mathcal{O}_0$ vanishes and this result simplifies for linearly polarized detection ($\beta = 0$) to

$$I(\phi, \theta, \chi) = \tfrac{1}{3}I_0\left\{1 - \tfrac{1}{2}h^{(2)}(J_i, J_f)\mathcal{A}_0\left[P_2(\cos\theta) - \tfrac{3}{2}\sin^2\theta\cos 2\chi\right]\right\}. \qquad 18.$$

Equation 18 can be utilized to design an experiment that measures the alignment $\mathcal{A}_0$ of an excited atomic or molecular fragment.

[1]We caution that the real second rank tensor $\mathcal{A}$ was defined by FM with a nonstandard normalization (83). For details of the transformation between collision and detector frames using real rotation matrices see Hertel & Stoll (84). We choose to retain the nonstandard normalization so that $\mathcal{A}_0$ ranges between 2 and -1 for any J_i (as does the asymmetry parameter β), and $\mathcal{A}_{1+}$ as well as $\mathcal{A}_{2+}$ range between -1 and 1. If a standard normalization is adopted, then the range of $\mathcal{A}_{1+}$ and $\mathcal{A}_{2+}$ must be multiplied by $\sqrt{3}$.

DETECTION OF LINEARLY POLARIZED LIGHT The most common method of determining the alignment is to detect light emitted at $\theta = 90°$ with respect to the collision axis z. The azimuthal angle ϕ is irrelevant in problems having a cylindrically symmetric collision frame, as may be seen in Eq. 18. The light intensities at two settings χ of the linear polarizer are required; these are most usually $I_{\parallel}$ $I_{\perp} = I(\phi, \frac{1}{2}\pi, \chi = \frac{1}{2}\pi)$. The "linear polarization" is then defined by

$$P = (I_{\parallel} - I_{\perp})/(I_{\parallel} + I_{\perp} \qquad 19.$$

and is related to the alignment by

$$P = 3h^{(2)}(J_i, J_f)\mathcal{A}_0/\left[4 + h^{(2)}(J_i, J_f)\mathcal{A}_0\right]. \qquad 20.$$

Thus the two quantities of interest, namely I_0 and $\mathcal{A}_0$, are determined by

$$I_0 = I_{\parallel} + 2I_{\perp}; \quad \mathcal{A}_0 = \frac{1}{h^{(2)}(J_i, J_f)} \frac{4P}{3-P}. \qquad 21.$$

Extraction of $\mathcal{A}_0$ is now possible, provided the light detected corresponds to a specific transition (branch) $J_i \to J_f$, using the values of $h^{(2)}(J_i, J_f)$ given in Table 1.

Often the experimentalist is not interested in the alignment, and wishes to measure I_0 alone. When this is the case, I_0 can be extracted from an intensity measurement at a *single* setting χ_M of the linear polarization analyzer; this is clearly an improvement on the method suggested by Eq. 21, requiring two measurements (of $I_{\parallel}$ and $I_{\perp}$). The so-called "magic angle" χ_M can be found by requiring the quantity multiplying $\mathcal{A}_0$ in Eq. 18 to vanish (85). Setting $\theta = \frac{1}{2}\pi$ for right angle photon observations as in Figure 2, the magic angle is given by the condition $\cos 2\chi_M = -\frac{1}{3}$, i.e. by

$$\chi_M = \cos^{-1}\left(\frac{1}{\sqrt{3}}\right) = 54.7°. \qquad 22.$$

At this setting the observed intensity is $I(\phi, \frac{1}{2}\pi, \chi_M) = \frac{1}{3}I_0$. If the right-angle detection geometry ($\theta = \frac{1}{2}\pi$) is inconvenient for some reason, a different magic angle $\chi_M(\theta)$ can be found for other observation directions θ. The general expression for the polarizer setting at which I is independent of $\mathcal{A}_0$ is then given by

$$\cos 2\chi_M(\theta) = \frac{(\cos^2\theta - \frac{1}{3})}{\sin^2\theta}, \qquad 23.$$

which has a solution only for $162.4° \geqslant \theta \geqslant 17.6°$.

DETECTION OF UNPOLARIZED LIGHT In some experiments, notably those in which the fluorescence photons are relatively energetic, it may not

prove practical to detect linearly polarized light. But the same information (I_0 and $\mathcal{A}_0$) can be found by detecting only unpolarized light, provided two detector positions θ are utilized. The intensity observed by a detector responding equally to arbitrary light polarization, i.e. having no polarization bias, is simply the sum of the $\chi = 0$ and $\chi = \frac{1}{2}\pi$ intensities in Eq. 18,

$$I_{unp}(\theta) = \tfrac{2}{3} I_0 \left[1 - \tfrac{1}{2} h^{(2)}(J_i, J_f) \mathcal{A}_0 \left(\tfrac{3}{2} \cos^2\theta - \tfrac{1}{2} \right) \right]. \qquad 24.$$

The intensity is independent of the alignment when θ is taken to be the magic angle 54.7°. While an intensity measurement at this value of θ suffices to determine I_0, one additional measurement is obviously needed to extract $\mathcal{A}_0$.

QUALITATIVE INTERPRETATION OF $\mathcal{A}_0$ To conclude this discussion of the cylindrically symmetric collision frame, we consider briefly the physical meaning of the alignment parameter $\mathcal{A}_0$. For definiteness, we denote the collision cross sections for producing excited states $|J_i M_i)$ by $\sigma(J_i M_i)$. Then $\mathcal{A}_0$ can be expressed as

$$\mathcal{A}_0 = \frac{\sum_{M_i} \left[3M_i^2 - J_i(J_i+1) \right] \sigma(J_i M_i)}{J_i(J_i+1) \sum_{M_i} \sigma(J_i M_i)}. \qquad 25.$$

Clearly $\mathcal{A}_0$ measures the relative populations of small $|M_i|$ states (with negative contributions to $\mathcal{A}_0$) versus large $|M_i|$ states (with positive contributions). If $\sigma(J_i M_i)$ is independent of M_i, then Eq. 25 shows that $\mathcal{A}_0 = 0$.

Thus $\mathcal{A}_0$ provides information on the nature of the spatial distribution of angular momentum vectors $\mathbf{J}_i$. This information is readily related to the shape of the excited state charge distribution. To illustrate this we treat in detail the example $J_i = 1$. Noting that $\sigma(J_i M_i) = \sigma(J_i, -M_i)$, and for convenience taking the $\sigma(J_i M_i)$ to be normalized, we have

$$\sigma(10) + 2\sigma(11) = 1. \qquad 26.$$

The alignment can now be evaluated using Eq. 25:

$$\mathcal{A}_0 = -1 + 3\sigma(11). \qquad 27.$$

By inverting Eq. 26 and Eq. 27, we can express the $\sigma(1M_i)$ in terms of $\mathcal{A}_0$ (this is only possible for $J_i = 1$, since the quadrupole moment is the highest multipole for a state with $J_i = 1$),

$$\sigma(1,0) = \tfrac{1}{3} - \tfrac{2}{3}\mathcal{A}_0; \quad \sigma(1,\pm 1) = \tfrac{1}{3} + \tfrac{1}{3}\mathcal{A}_0. \qquad 28.$$

Now, the $\sigma(1M_i)$ also determine the average excited state charge density

of, for example, a one-electron atom through

$$\rho \propto \sum_{M_i} \left| Y_{J_i M_i}(\theta, \phi) \right|^2 \sigma(J_i M_i). \qquad 29.$$

For our example with $J_i = 1$ then, the angular variation of the charge distribution is given by

$$\rho \propto 1 - 2\mathcal{A}_0 P_2(\cos\theta). \qquad 30.$$

Thus if $\mathcal{A}_0 = 0$, the charge distribution is isotropic. If $\mathcal{A}_0 < 0$, ρ becomes elongated along the collision axis z. Finally if $\mathcal{A}_0 > 0$, ρ becomes flattened along the collision axis. These three alternatives are depicted qualitatively in Figure 4.

Breakdown of Cylindrical Symmetry

Next we consider experiments of greater complexity, possessing a *plane* of symmetry only (53, 83, 84, 86–89). This plane is taken by convention to be the xz-plane in the collision frame. All tensor elements (multipole moments) not symmetric under the transformation $y \to -y$ vanish identically. Restricting ourselves again to the usual class of experiments in which the collision partners have no net helicity (preferred spin direction), this leaves three elements of the alignment tensor and one element of the

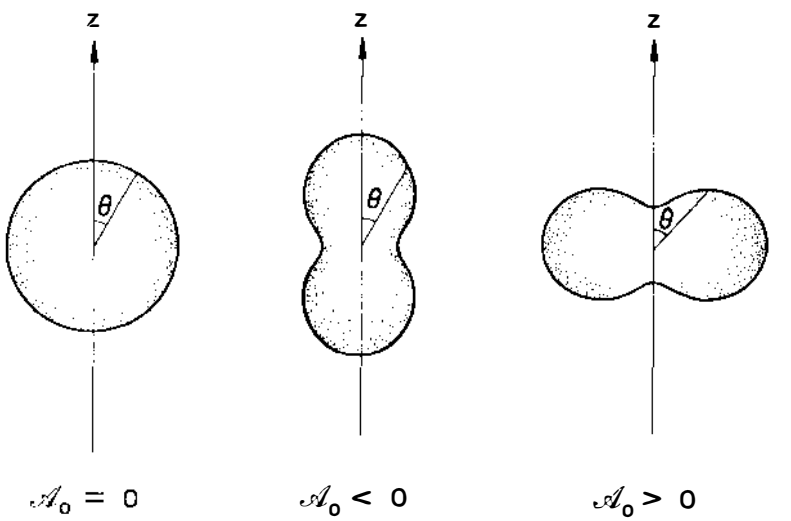

Figure 4 Form of the charge distribution $\rho(\theta)$ as a function of the alignment parameter $\mathcal{A}_0$.

orientation vector:

$$\begin{aligned}
\mathcal{A}_0 &= \langle (J_i|3J_z^2 - \mathbf{J}^2|J_i)\rangle / J_i(J_i+1),\\
\mathcal{A}_{1+} &= \langle (J_i|J_xJ_z + J_zJ_x|J_i)\rangle / J_i(J_i+1),\\
\mathcal{A}_{2+} &= \langle (J_i|J_x^2 - J_y^2|J_i)\rangle / J_i(J_i+1),\\
\mathcal{O}_{1-} &= \mathcal{O}_y = \langle (J_i|J_y|J_i)\rangle / \sqrt{J_i(J_i+1)}\,. \qquad 31.
\end{aligned}$$

Here $\mathcal{O}_{1-}$ is simply the standard tensor notation for the y-component of the pseudovector $\mathcal{O}$. Note that $\mathcal{A}_0$, $\mathcal{A}_{1+}$, and $\mathcal{A}_{2+}$ are manifestly symmetric under the transformation $y \to -y$. By this reasoning it might appear that $\mathcal{O}_y$ is odd, but we must be careful to properly account for the pseudovector nature of $\mathcal{O}$. One simple way to do this is to rewrite the components of $\mathcal{O}$ as quadratic operators in $\mathbf{J}$, utilizing the commutation rules $i\hbar\mathbf{J} = \mathbf{J}\times\mathbf{J}$. Then we see explicitly that

$$\begin{aligned}
&J_y = (J_zJ_x - J_xJ_z)/i\hbar, \qquad J_x = (J_yJ_z - J_zJ_y)/i\hbar,\\
&J_z = (J_xJ_y - J_yJ_x)/i\hbar, \qquad 32.
\end{aligned}$$

which makes it clear that only $\mathcal{O}_y$ is even under the transformation $y \to -y$.

RELATIONSHIP BETWEEN DETECTOR AND COLLISION FRAME MULTIPOLES

As discussed in FM, these four anisotropy elements describe the distribution of polarized fluorescence. While the intensity expression (Eq. 13) in the detector frame is unchanged, the relationship between the detector- and collision-frame alignment and orientation is more complicated than for a cylindrically symmetric collision frame. This relationship, corrected for some misprints in the original article of Fano & Macek, is given by:

$$\begin{aligned}
\mathcal{A}_0^{\text{det}} &= \mathcal{A}_0 P_2(\cos\theta) + \mathcal{A}_{1+}\left(\tfrac{3}{2}\sin 2\theta\cos\phi\right) + \mathcal{A}_{2+}\left(\tfrac{3}{2}\sin^2\theta\cos 2\phi\right);\\
\mathcal{A}_{2+}^{\text{det}} &= \mathcal{A}_0\left(\tfrac{1}{2}\sin^2\theta\cos 2\chi\right)\\
&\quad + \mathcal{A}_{1+}(\sin\theta\sin\phi\sin 2\chi - \sin\theta\cos\theta\cos\phi\cos 2\chi)\\
&\quad + \mathcal{A}_{2+}\left[\tfrac{1}{2}(1+\cos^2\theta)\cos 2\phi\cos 2\chi - \cos\theta\sin 2\phi\sin 2\chi\right];\\
\mathcal{O}_0^{\text{det}} &= \mathcal{O}_{1-}\sin\theta\sin\phi. \qquad 33.
\end{aligned}$$

By inserting Eq. 33 into Eq. 13 the general expression for spatial variations of the polarized fluorescence is obtained (we do not bother to write it down here).

EXPERIMENTAL DETERMINATION OF $\mathcal{A}$ AND $\mathcal{O}$ It is instructive to compare the preceding analysis with the more common method of analyzing polarized light. Any beam of light can be completely characterized, as is well known (90, 91), by four Stokes parameters I, M, C, and S. The emitted light distribution predicted by Eq. 13 and Eq. 33 depends on the total intensity I_0 and on four anisotropy elements $(\mathcal{A}_0, \mathcal{A}_{1+}, \mathcal{A}_{2+}, \mathcal{O}_{1-})$, making a total of five independent parameters. It should not be surprising that this treatment requires more dynamical parameters than the Stokes treatment, since Eq. 13 and Eq. 33 essentially predict the Stokes parameters associated with a light beam emitted into *any* direction (θ, ϕ) of space. Consequently we reach an important conclusion:

> all anisotropy parameters cannot be determined by polarization measurements made with a detector fixed in only one direction of space (θ, ϕ).

This implies that determination of $\mathcal{A}_0$, $\mathcal{A}_{1+}$, $\mathcal{A}_{2+}$, and $\mathcal{O}_{1-}$ is far more difficult experimentally than is the determination of $\mathcal{A}_0$ in cylindrically symmetric problems, which requires only two intensity measurements with a linear polarizer and a fixed detector. Even so, this remains far simpler than a collision frame without even a plane of symmetry, which can have nine nonvanishing quantities, five elements of $\mathcal{A}$, three elements of $\mathcal{O}$ and, of course, I_0.

It should be pointed out that the expressions 13 and 33 given above for the emitted light distribution apply to any type of excitation process having a plane of symmetry (89). However, when the excitation *is* produced by photofragmentation of nonoriented (92–95) targets using either linearly polarized or unpolarized incident light, $\mathcal{O}_{1-}$ is identically zero owing to symmetry under $\hat{\mathbf{z}} \rightarrow -\hat{\mathbf{z}}$. A consideration of chiral targets can be found elsewhere (96–98).

Depolarization Caused by Unresolved Structure

The preceding formulation has treated light emission by an atom or molecule from a state of well-defined angular momentum $\mathbf{J}_i$. When light is emitted from two or more closely lying levels that are coherently excited, this formulation must be modified. Figure 5 illustrates qualitatively the reason for this added complexity. That is, the two or more paths leading from the initial photofragmentation to the final photon detection are indistinguishable, at least when the detector resolution cannot distinguish $h\nu_{ac}$ from $h\nu_{bc}$. Accordingly, the intensity is the absolute square of a coherent summation over the amplitudes for all indistinguishable pathways a,b,..., and the intensity may exhibit

"quantum beats": cross terms which oscillate in the time t of photon emission after the fragmentation as $\cos[(E_a - E_b)t/\hbar]$ (99).

The quantitative treatment of such nonstationary states requires, in general, the solution to the full time-dependent Schroedinger equation as a function of t. While this may prove in general to be a difficult problem, Fano & Macek have found a very simple formulation that is applicable when the energy splittings of interest are caused by hyperfine structure (77, 100, 101). They show that the hyperfine structure induces a time dependence in all of the multipole moments according to

$$\mathcal{Q}(t) = \mathcal{Q}(0)g^{(2)}(t),$$
$$\mathcal{O}(t) = \mathcal{O}(0)g^{(1)}(t), \qquad 34.$$

where

$$g^{(k)}(t) = \sum_{F,F'} \frac{(2F+1)(2F'+1)}{(2I+1)} \begin{Bmatrix} F & F' & k \\ J_i & J_i & I \end{Bmatrix}^2 \cos \omega_{F'F} t. \qquad 35.$$

Here $\omega_{F'F}$ is the frequency splitting between two hyperfine levels whose total angular momenta are $\mathbf{F}'$ and $\mathbf{F}$, J_i is the excited state angular momentum quantum number, and I is the nuclear spin.

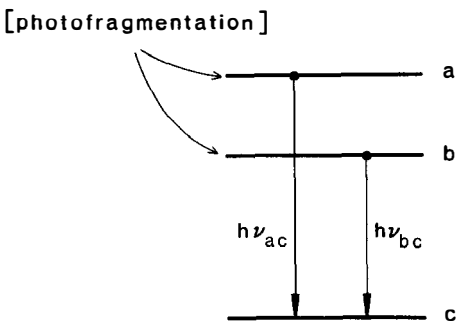

Figure 5 Diagram of two indistinguishable paths whose amplitudes add coherently and cause quantum beats. In the photofragmentation process pictured, two levels a and b are populated and locked together in phase (coherently excited). They both radiate to the same final level c. Then the intensity is proportional to the square of the sum of the probability amplitudes associated with each individual path, i.e. to $|\langle c|\hat{\mathcal{E}}\cdot\mathbf{r}|a\rangle + \langle c|\hat{\mathcal{E}}\cdot\mathbf{r}|b\rangle|^2$. The cross term may contribute constructively or destructively to the total transition rate, causing an interference effect, called quantum beats, to appear in the intensity observed at some fixed location in space by a detector that responds to both $h\nu_{ac}$ and $h\nu_{bc}$. If $|a(t)\rangle = |a(0)\rangle\exp(-iE_a t/\hbar)$ and $|b(t)\rangle = |b(0)\rangle\exp(-iE_b t/\hbar)$, then the cross term shows a time dependence proportional to $\cos(E_a - E_b)t/\hbar$ with a beat frequency equal to the energy difference between the levels divided by Planck's constant.

Despite the somewhat complicated appearance of Eq. 35, it has a simple physical interpretation. At $t=0$, the fragmentation process is usually assumed to align and orient the electronic charge cloud only. As the time t increases, the angular momentum operator $\mathbf{J}$, whose components determine $\mathcal{A}$ and $\mathcal{O}$, are no longer constants of the motion. Instead $\mathbf{J}$ and $\mathbf{I}$ precess about $\mathbf{F}$, causing the electronic and nuclear multipole moments to oscillate back and forth. This qualitative view is supported by the fact that $g^{(k)}(t)$ attains its maximum value, unity, at $t=0$. Accordingly, we interpret $\mathcal{A}(0)$ and $\mathcal{O}(0)$ as the *electronic* contributions to the alignment and orientation.

Most experiments do not achieve the time resolution required to observe the oscillations implied by Eq. 35. To use this result in the context of time-unresolved measurements, we integrate over all time including an exponential decay factor $\exp(-t/\tau)$ for the total intensity. This gives

$$\langle \mathcal{A}(t)\rangle = \mathcal{A}(obs) = \mathcal{A}(0)\bar{g}^{(2)},$$
$$\langle \mathcal{O}(t)\rangle = \mathcal{O}(obs) = \mathcal{O}(0)\bar{g}^{(1)}, \qquad 36.$$

where the time-averaged value of $g^{(k)}(t)$ is given by

$$\bar{g}^{(k)} = \sum_{F,F'} \frac{(2F+1)(2F'+1)}{(2I+1)} \begin{Bmatrix} F & F' & k \\ J_i & J_i & I \end{Bmatrix}^2 \frac{1}{1+\omega_{F'F}^2\tau^2} \qquad 37.$$

in which each factor $\cos\omega_{F'F}t$ is replaced by $(1+\omega_{F'F}^2\tau^2)^{-1}$. The "depolarization factor" $\bar{g}^{(k)}$ lies between two extremes:

1. $|\omega_{F'F}| \ll \tau^{-1}$. In this limit the precession of $\mathbf{J}$ about $\mathbf{F}$ is so slow that essentially no precession occurs before the light is emitted. Then $\bar{g}^{(k)} \approx 1$ and the unresolved oscillations have no depolarizing effect.

2. $|\omega_{F'F}| \gg \tau^{-1}$. In this limit the precession is rapid and $\mathbf{J}$ precesses about $\mathbf{F}$ many times before the light is emitted. Then all terms with $F' \neq F$ vanish and the observed alignment $\mathcal{A}(obs)$ or orientation $\mathcal{O}(obs)$ is reduced from the actual electronic alignment or orientation by the factor

$$\bar{g}^{(k)} \approx \sum_F \frac{(2F+1)^2}{(2I+1)} \begin{Bmatrix} F & F & k \\ J_i & J_i & I \end{Bmatrix}^2. \qquad 38.$$

But if $J_i \gg I$, as is typical of molecular problems, this depolarization factor is still close to unity because the precession has little effect on the direction of $\mathbf{J}_i$. In this limit the squared $6j$-coefficient is approximately given in terms of a Legendre polynomial and

$$\bar{g}^{(k)} \underset{J_i,\, F \gg I}{\longrightarrow} \sum_F \frac{2F+1}{2I+1} \frac{[P_k(\hat{\mathbf{J}}_i\cdot\hat{\mathbf{F}})]^2}{(2J_i+1)}, \qquad 39.$$

which approaches 1 as $\hat{\mathbf{J}}_i \cdot \hat{\mathbf{F}}$ approaches unity. When $I \approx J_i$ a sizeable depolarization can occur, as demonstrated for atoms by Hafner, Kleinpoppen & Krüger (102).

Often, in light emission by molecules, the hyperfine precession is negligibly slow on the time scale of the radiative lifetime τ. Then case 1 applies and the hyperfine depolarization effect can be neglected. It remains possible, however, that the light emission from members of a fine structure multiplet is unresolved. In such a case the preceding formulation still applies, provided we make the substitutions $I \to S$, $F, F' \to J_i, J_i'$, and $J_i \to N$, where $\mathbf{N}$ is the orbital angular momentum of the molecule and $\mathbf{S}$ is its spin. Then $\mathcal{Q}(0)$ and $\mathcal{O}(0)$ are purely *orbital* multipoles.

ANGULAR MOMENTUM TRANSFER TREATMENT OF PHOTOFRAGMENTATION

We turn to a detailed analysis of the dynamical information contained in the alignment and orientation of photofragments. In the section above we emphasize the importance of separating the fragmentation dynamics, contained solely in $\mathcal{Q}_0$ and $\mathcal{O}_0$ for cylindrically symmetric problems, from geometrical aspects of dipole radiation emission. In this section we develop this point of view one step further, by showing how $\mathcal{Q}_0$ and $\mathcal{O}_0$ can themselves be analyzed into the following:

1. a geometrical contribution reflecting only the dipole nature of the photofragmentation process;
2. a few amplitudes containing all dynamical information that it is possible to learn from fluorescence polarization measurements.

Angular Momentum Transfer Formalism

The most obvious way to specify the probability for any given photofragmentation process is in terms of continuum amplitudes specified in *jj*-coupling. In the following we consider only processes of the type

$$h\nu(j_{ph}=1)+AB(J_0)\to[A(j_i)+B(s)](\ell). \qquad 40.$$

Here we have indicated a photon carrying one unit of angular momentum incident on a molecule AB (not necessarily a diatomic) with angular momentum $\mathbf{J}_0$. The fragments A and B so produced have internal angular momenta $\mathbf{j}_i$ and $\mathbf{s}$, respectively, and the orbital angular momentum of the A–B composite system is ℓ. For photodissociation experiments, in which B can be an atom or molecule, $\mathbf{s}$ is its total angular momentum, whereas in photoionization experiments B is a photoelectron with spin quantum number $s=\frac{1}{2}$. The partial cross section for producing fragments A in

some state with angular momentum $\mathbf{j}_i$ is determined by a reduced dipole matrix element between the initial (bound) state and the final (continuum) state with total angular momentum $\mathbf{J}$,

$$\sigma(j_i) \quad C_0 \sum_{s,\ell,j_s,J} \left|\left(j_i(s\ell)j_sJ \,\|\, r^{(1)} \,\|\, J_0\right)\right|^2. \qquad 41.$$

In Eq. 41, C_0 is a constant proportional to the photon energy, which is irrelevant for our analysis, and $\mathbf{j}_s = \boldsymbol{\ell} + \mathbf{s}$ is the sum of all fragment angular momenta in the final state that are not observed. The final state wave function is assumed to be energy-normalized, and to satisfy the incoming-wave boundary condition at large fragment separations $r_{AB} \to \infty$.

Recall that the polarization of light emitted by fragment A in a dipole transition $j_i \to j_f$ depends on the partial cross section $\sigma(j_i m_i)$ for leaving A in a state with magnetic quantum number m_i. Unlike Eq. 41 for $\sigma(j_i)$, however, $\sigma(j_i m_i)$ involves a coherent summation over J, (i.e. cross terms with $J \neq J'$) even though the summations over s, ℓ, and j_s remain incoherent. Physically, this expresses the fact that the operators $\mathbf{J}^2$ and j_{iz} do not commute.

The main idea of the angular momentum transfer formulation, as used long ago by Fano (103), and as extensively developed more recently by Dill & Fano (78–80), is that any fragment anisotropy should be analyzed in terms of a new set of continuum amplitudes. The new amplitudes are characterized not by the total angular momentum $\mathbf{J}$, but by $\mathbf{j}_t$, the unobserved angular momentum transferred from the target to the photofragments. When so defined, $\mathbf{j}_t^2$ commutes with the angular momenta associated with the observed anisotropy, and hence the contributions to the anisotropy from each $\mathbf{j}_t$ add incoherently.

Applications of this approach have been restricted until very recently to angular distributions of photofragments, in which case the observed angular momentum is $\boldsymbol{\ell}$ and the angular momentum transfer is given by $\mathbf{j}_i + \mathbf{s} - \mathbf{J}_0 = \mathbf{j}_{ph} - \boldsymbol{\ell}$. Dill et al (72) first applied this method to our present problem of photofragment alignment, defining a different angular momentum transfer according to

$$\mathbf{j}_t = \boldsymbol{\ell} + \mathbf{s} - \mathbf{J}_0 = \mathbf{j}_{ph} - \mathbf{j}_i. \qquad 42.$$

Klar (56, 57) has also applied an angular momentum transfer formalism to treat this problem but with a different definition of $\mathbf{j}_t$. As discussed by D. Dill in unpublished correspondence with R. N. Zare in 1977, and as amplified by Greene & Zare (59), the new continuum amplitudes S are

related to the old ones by

$$S(J_0, s, \ell, j_s, j_i; j_t) = \sum_J \left(\frac{2j_t+1}{3}\right)^{1/2} \begin{Bmatrix} j_i & j_s & J \\ J_0 & \ell & j_t \end{Bmatrix} \times \left(j_i(s\ell)j_s J \| r^{(1)} \| J_0\right). \qquad 43.$$

To within normalization, this results in the incoherent summation

$$\sigma(j_i m_i) = \sum_{s,\ell,j_s,j_t} |S(J_0, s, \ell, j_s, j_i; j_t)|^2 (j_i m_i, j_t q - m_i | 1 q)^2. \qquad 44.$$

Here q is the component of incident photon angular momentum along the quantization axis $\hat{\mathbf{z}}$, i.e. the photon helicity. Linearly polarized incident light thus has $q=0$, unpolarized light is the average of $q=\pm 1$, and left-circularly polarized light has $q=+1$.

Equation 44 shows how the m_i dependence of $\sigma(j_i m_i)$ for each j_t arises only through Wigner coefficients (Clebsch-Gordan coefficients). Consequently, the alignment $\mathcal{A}_0$ and orientation $\mathcal{O}_0$ contributed by each j_t can be evaluated in closed form. We have found that

$$\mathcal{A}_0(j_i) = \sum_{j_t} |S(j_i; j_t)|^2 \mathcal{A}_0(j_i; j_t) \Big/ \sum_{j_t} |S(j_i; j_t)|^2,$$

$$\mathcal{O}_0(j_i) = \sum_{j_t} |S(j_i; j_t)|^2 \mathcal{O}_0(j_i; j_t) \Big/ \sum_{j_t} |S(j_i, j_t)|^2, \qquad 45.$$

where

$$|S(j_i; j_t)|^2 = \sum_{s,l,j_s} |S(J_0, s, \ell, j_s, j_i; j_t)|^2, \qquad 46.$$

and the summation over j_t is restricted to the three values $j_i - 1$, j_i, and $j_i + 1$. In Eq. 45 we have introduced two universal functions describing the alignment $\mathcal{A}_0(j_i; j_t)$ and orientation $\mathcal{O}_0(j_i; j_t)$ arising from each transfer j_t. These are given in Table 2, where the dependence on q is shown explicitly. Note that $\mathcal{A}_0$ for circularly polarized ($q=\pm 1$) or for unpolarized incident light is simply minus one-half the value of $\mathcal{A}_0$

[2]More generally, elliptically polarized incident radiation can be shown to excite two nonzero alignment parameters, $\mathcal{A}_0$ and $\mathcal{A}_{2+}$. These are referred to a coordinate system in which the photon beam is incident along $\hat{\mathbf{z}}$ and the major and minor axes of the ellipse coincide with $\hat{x}$ and $\hat{y}$ in Figure 3. If the alignment obtained using linearly polarized incident radiation is denoted $\mathcal{A}_0^{\text{lin}}$, then the alignment parameters obtained using elliptically polarized radiation are given by $\mathcal{A}_0 = -\frac{1}{2}\mathcal{A}_0^{\text{lin}}$, $\mathcal{A}_{1+} = 0$, $\mathcal{A}_{2+} = -\frac{1}{2}p\mathcal{A}_0^{\text{lin}}$. Here $p = (I_y - I_x)/(I_y + I_x)$ is the linear polarization of the incident radiation.

Table 2 The universal orientation and alignment factors $\mathcal{O}_0(j_i;\, j_t)$ and $\mathcal{A}_0(j_i;\, j_t)$, where the dependence on the incident photon helicity, q, has been made explicit

j_t	Absorption branch	$\mathcal{O}_0(j_i;\, j_t, q)$	$\mathcal{A}_0(j_i;\, j_t, q)$
j_i+1	$P\uparrow$	$-\dfrac{\frac{1}{2}qj_i}{\sqrt{j_i(j_i+1)}}$	$-(-1)^q(1-\frac{1}{2}q^2)\dfrac{2j_i-1}{5(j_i+1)}$
j_i	$Q\uparrow$	$\dfrac{\frac{1}{2}q}{\sqrt{j_i(j_i+1)}}$	$(-1)^q(1-\frac{1}{2}q^2)\dfrac{(2j_i-1)(2j_i+3)}{5j_i(j_i+1)}$
j_i-1	$R\uparrow$	$\dfrac{\frac{1}{2}q(j_i+1)}{\sqrt{j_i(j_i+1)}}$	$-(-1)^q(1-\frac{1}{2}q^2)\dfrac{2j_i+3}{5j_i}$

obtained with linearly polarized light ($q=0$).[2] These results for the alignment were presented before (59), but have not been given previously for the orientation.

The three alternative values of $h^{(2)}(j_i, j_f)$ in Table 1, coupled with the three values of $\mathcal{A}_0(j_i;\, j_t)$ in Table 2, determine nine limiting cases for the linear polarization in the high j_i limit through Eq. 20. These yield exactly the same results as found by Macpherson, Simons & Zare (14).

Dependence of the Universal Alignment and Orientation Functions on Parity-Favoredness

The values of the universal alignment function $\mathcal{A}_0(j_i;\, j_t)$ are plotted in Figure 6, while those of the universal orientation function $\mathcal{O}_0(j_i;\, j_t)$ are shown in Figure 7. The alignment contributions associated with angular momentum transfers $j_t \neq j_i$ are negative, while those with $j_t = j_i$ are positive. In addition, the two alignment curves with $j_t \neq j_i$ converge as $j_i \to \infty$ to the same value $-2/5$, while the curve $\mathcal{A}_0(j_i;\, j_i)$ approaches $4/5$ in the same limit. These results suggest strongly that contributions to the fragmentation having transfers $j_t \neq j_i$ differ qualitatively from contributions from transfers $j_t = j_i$. This qualitative difference can be traced to the *parity-favoredness quantum number* π_f, which is either $+1$ or -1 for each angular momentum transfer (104). In general π_f is defined by

$$\pi_f = (-1)^{j_t - j_{obs} + j_{ph}} = (-1)^{j_t - j_{obs} + 1}, \qquad 47.$$

which reduces in the present problem with $j_{obs} = j_i$ to

$$\pi_f = (-1)^{j_t - j_i + 1} = \begin{cases} +1, & j_t \neq j_i \quad \text{(parity-favored)} \\ -1, & j_t = j_i \quad \text{(parity-unfavored)}. \end{cases} \qquad 48.$$

The sign of the alignment is thus solely determined by the parity-favoredness.

An analogous result was first derived for the photofragment angular distribution asymmetry parameter β by Dill & Fano (79). [The definition of β is given in Eq. 1, and is not the same β of Eq. 12]. In particular, for photofragmentation experiments using linearly polarized incident photons, the parity-unfavored contributions to β are identically -1. Parity-favored contributions to β can instead range anywhere from -1 to 2, depending on the specific dynamics of the problem, with experience showing that they tend to be positive. We should point out that whereas the alignment contribution of each transfer can be evaluated in closed form (Table 2) independently of dynamical considerations, the same is not true for β. This stems from the fact that j_i, the "observed" angular momentum quantum in alignment measurements, has only one value, while the observed angular momentum in angular distribution measurements is ℓ, which can range over many values.

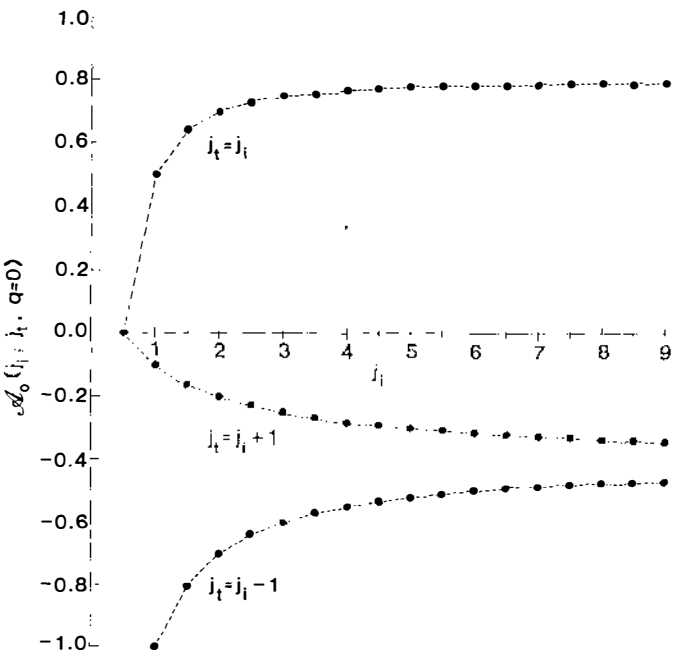

Figure 6 Plot of the universal alignment function $\mathscr{A}_0(j_i; j_t)$ for linearly polarized incident light ($q = 0$) as a function of the photofragment angular momentum quantum number j_i and the angular momentum transfer quantum number j_t. Contrast the behavior of the parity-favored ($j_t \neq j_i$) and parity-unfavored ($j_t = j_i$) contributions. For circularly polarized ($q = \pm 1$) or unpolarized incident light, the values are to be multiplied by $-\frac{1}{2}$.

In the case of photoionization in which the ejected particle (electron) is the same as the collection of particles the electric vector of the light beam acts upon, the sign of either second rank anisotropy (i.e. β or $\mathcal{A}_0$) provides an indication of whether the fragmentation is a simple, direct break-up process. To see this connection, we consider the two possible limits for the coefficient of $P_2(\cos\theta)$, which is β in Eq. 1 and $-2\mathcal{A}_0$ in Eq. 30. The upper limit for β is 2, for which the photofragmentation axis $\hat{\mathbf{k}}$ peaks along the incident polarization axis $\hat{\mathcal{E}}$:

$$d\sigma/d\Omega \propto |\hat{\mathcal{E}}\cdot\hat{\mathbf{k}}|^2. \qquad 49.$$

Similarly, Eq. 30 and Figure 4 show that when $-2\mathcal{A}_0 = 2$, the charge density is elongated along the polarization vector also. This is the pattern expected for *direct* processes, which tend to pull the fragments apart along the direction of the force that is exerted on the target by the photon electric field. These are the parity-favored processes. In the opposite extreme, the coefficient of $P_2(\cos\theta)$ is -1, and the photofrag-

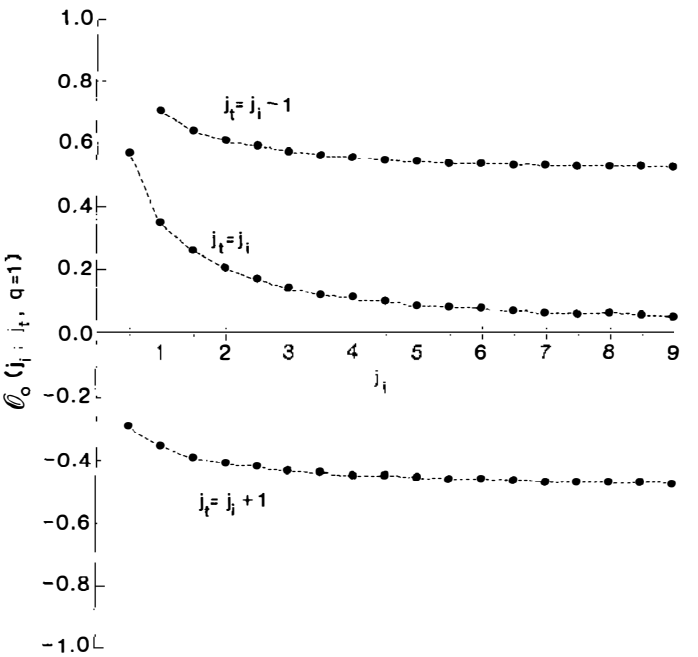

Figure 7 Plot of the universal orientation function $\mathcal{O}_0(j_i; j_t)$ for left-circularly polarized incident light ($q = 1$) as a function of the photofragment angular momentum quantum number j_i and the angular momentum transfer quantum number j_t. For right-circularly polarized light the values are multiplied by -1, while for linearly polarized light or unpolarized light they vanish.

mentation peaks at right angles to $\hat{\mathfrak{E}}$:

$$d\sigma/d\Omega \propto |\hat{\mathfrak{E}} \times \hat{\mathbf{k}}|^2. \qquad 50.$$

Similarly, the charge density is elongated orthogonally to $\hat{\mathfrak{E}}$ when $-2\mathcal{A}_0 = -1$. The observation of such an angular distribution or alignment is far more interesting and less common than the pattern in Eq. 49, and is the signature of screw-type interactions between the fragments (79, 105–107). A simple classical analogy of each type of fragmentation process is provided by an implusive force **F** delivered radially to an object resting on a merry-go-round (11, 108). If the merry-go-round is stationary or rotating slowly, the object is ejected axially along **F** (axial recoil), but if the merry-go-round initially is rotating rapidly, then the object is ejected tangentially, perpendicular to **F** (transverse recoil). The latter type of fragmentation process is generally associated with parity-unfavored angular momentum transfers.[3]

In the case of photodissociation, the initial recoil direction of the nuclei has in general some fixed orientation with respect to the electron cloud, for example, along the electronic transition moment for a parallel-type transition or at right angles to the electronic transition moment for a perpendicular-type transition. With suitable modification, the connection between parity favoredness or unfavoredness and axial or transverse recoil exactly carries over.

The manner in which these ideas apply to fragment orientation is perhaps less obvious, as the parity-favored and unfavored terms of the universal function $\mathcal{O}_0(j_i; j_t)$ plotted in Figure 7 do not have opposite signs. It is apparent, however, that parity-favored and parity-unfavored contributions to $\mathcal{O}_0(j_i)$ are qualitatively different. That is, $\mathcal{O}_0(j_i; j_t) \to 0$ as $j_i \to \infty$ for the parity-unfavored transfer $j_t = j_i$, while $\mathcal{O}_0(j_i; j_t) \to \pm 1/2$ for the parity-favored transfers $j_t = j_i \mp 1$.

Extraction of Dynamical Information from Measurements of $\mathcal{A}_0$ and $\mathcal{O}_0$

Equations 45 and 46, along with Table 2, represent a focal point of this article. They show how the fragment alignment and orientation are generally the incoherent average of three alternative values of the transfer j_t. Moreover, Eq. 45 fully disentangles the fragmentation dynamics, contained in $S(j_i; j_t)$, from the geometrical considerations, contained in

[3]While this is strictly true of the *alignment* pattern, there are examples of parity-favored angular momentum transfers which nonetheless give rise to *angular distributions* of the orthogonal type shown in Eq. 50. These exceptions are sometimes termed "dynamically unfavored." They originate from the coherent contribution to the anisotropy of more than one value of j_{obs}. See Greene (106) and Fano & Greene (107).

the universal functions for the alignment $\mathcal{A}_0(j_i; j_t)$ and the orientation $\mathcal{O}_0(j_i; j_t)$.

Let us introduce the three normalized quantities

$$\mathcal{S}_+ = \frac{|S(j_i; j_i+1)|^2}{\sum_{j_t} |S(j_i; j_t)|^2},$$

$$\mathcal{S}_0 = \frac{|S(j_i; j_i)|^2}{\sum_{j_t} |S(j_t; j_t)|^2},$$

and

$$\mathcal{S}_- = \frac{|S(j_i; j_i-1)|^2}{\sum_{j_t} |S(j_i; j_t)|^2}, \qquad 51.$$

which may be interpreted as the fraction of each angular momentum transfer contributing to the photofragmentation process. We call the $\mathcal{S}$ the angular momentum transfer channel probabilities. Because $\mathcal{S}_+ + \mathcal{S}_0 + \mathcal{S}_- = 1$, only two of these dynamical quantities are independent. Then Eqs. 45 and 46 may be rewritten as

$$\mathcal{A}_0(j_i) = \mathcal{S}_+\mathcal{A}_0(j_i; j_i+1) + \mathcal{S}_0\mathcal{A}_0(j_i; j_i) + \mathcal{S}_-\mathcal{A}_0(j_i; j_i-1);$$
$$\mathcal{O}_0(j_i) = \mathcal{S}_+\mathcal{O}_0(j_i; j_i+1) + \mathcal{S}_0\mathcal{O}_0(j_i; j_i) + \mathcal{S}_-\mathcal{O}_0(j_i; j_i-1). \qquad 52.$$

Thus the three channel probabilities $\mathcal{S}$ represent *all* the dynamical information one can learn about a given photofragmentation process by measuring the polarization of light emitted by one fragment.

In the most common photofragment emission studies only the alignment $\mathcal{A}_0(j_i)$ is measured. Although it is not possible to deduce the individual channel probabilities, this does provide some measure of the ratio of parity-unfavored to parity-favored contributions. Indeed in limit of large j_i, Figure 6 shows how $\mathcal{A}_0(j_i; j_i+1)$ and $\mathcal{A}_0(j_i; j_i-1)$ both approach the same value $(-2/5)$. Thus in the high j_i limit, a measurement of $\mathcal{A}_0$ alone gives directly the ratio

$$\gamma = \frac{\mathcal{S}_0}{\mathcal{S}_+ + \mathcal{S}_-} = \frac{|S(j_i; j_i)|^2}{|S(j_i; j_i+1)|^2 + |S(j_i; j_i-1)|^2}. \qquad 53.$$

This parametric dependence of $\mathcal{A}_0$ on γ is illustrated in Figure 8, which may facilitate the interpretation of experimental data in the limit of large j_i.

Knowledge of $\mathcal{A}_0$ and $\mathcal{O}_0$ provides sufficient information to extract all three channel probabilities. For example, a measurement of $\mathcal{A}_0$ and $\mathcal{O}_0$

using left circularly polarized incident light can be inverted, giving

$$\mathcal{S}_+ = \frac{5}{3}\frac{j_i}{2j_i+1}\mathcal{A}_0(j_i) - \frac{(2j_i+3)\sqrt{j_i(j_i+1)}}{(j_i+1)(2j_i+1)}\mathcal{O}_0(j_i) + \frac{2j_i+3}{3(2j_i+1)};$$

$$\mathcal{S}_- = \frac{5}{3}\frac{j_i+1}{2j_i+1}\mathcal{A}_0(j_i) + \frac{(2j_i-1)\sqrt{j_i(j_i+1)}}{j_i(2j_i+1)}\mathcal{O}_0(j_i) + \frac{2j_i-1}{3(2j_i-1)};$$

$$\mathcal{S}_0 = -\frac{5}{3}\mathcal{A}_0(j_i) - \frac{\mathcal{O}_0(j_i)}{\sqrt{j_i(j_i+1)}} + \frac{1}{3}. \qquad 54.$$

Note the simple form the channel probabilities attain in the high j_i limit, but that for smaller values of j_i Eq. 54 must be used in full. We regard the

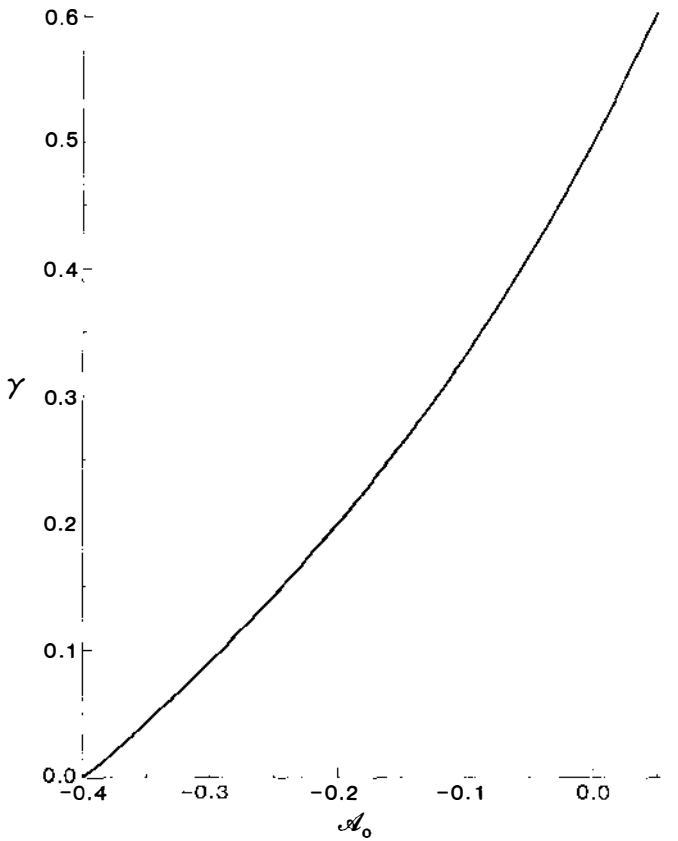

Figure 8 The dependence of γ, the ratio of parity-unfavored to the sum of parity-favored channel probabilities, on $\mathcal{A}_0$, the value of the alignment parameter in the high j_i limit. The actual function plotted is $\gamma = (5\mathcal{A}_0 + 2)/(4 - 5\mathcal{A}_0)$.

extraction of these angular momentum transfer channel probabilities as the primary goal for this class of experiments.

ACKNOWLEDGMENTS

We thank R. Bersohn, P. J. Brucat, C. D. Caldwell, and G. W. Loge for critically reading earlier drafts of this manuscript. This work was supported by grants from the National Science Foundation.

Literature Cited

1. Simons, J. P. 1977. *Gas Kinetics and Energy Transfer, Chem. Soc. Spec. Period. Rep.* 2:58–95
2. Gelbart, W. M. 1977. *Ann. Rev. Phys. Chem.* 28:323–48
3. Okabe, H. 1978. *Photochemistry of Small Molecules.* New York: Wiley. 431 pp.
4. Leone, S. R. 1982. *Adv. Chem. Phys.* 50:255–324
5. Berkowitz, J. 1979. *Photoabsorption, Photoionization, and Photoelectron Spectroscopy.* New York: Academic. 469 pp.
6. Fano, U., Cooper, J. W. 1968. *Rev. Mod. Phys.* 40:441–507
7. Pratt, R. H., Ron, A., Tseng, H. K. 1973. *Rev. Mod. Phys.* 45:273–325, 663
8. Samson, J. A. R. 1982. *Handb. Phy.* 31: In press
9. Bersohn, R., Lin, S. H. 1969. *Adv. Chem. Phys.* 16:67–100
10. Jonah, C. 1971. *J. Chem. Phys.* 55:1915
11. Zare, R. N. 1972. *Mol. Photochem.* 4:1–37
12. Yang, S. C., Bersohn, R. 1974. *J. Chem. Phys.* 61:4400–7
13. Dzvonik, M. J., Yang, S., Bersohn, R. 1974. *J. Chem. Phys.* 61:4408–21
14. Macpherson, M. T., Simons, J. P., Zare, R. N. 1979. *Mol. Phys.* 38:2049–55
15. Band, Y. B., Freed, K. F., Kouri, D. J. 1981. *Chem. Phys. Lett.* 79:233–37
16. Band, Y. B., Freed, K. F. 1981. *Chem. Phys. Lett.* 79:238–43
17. Band, Y. B., Freed, K. F., Kouri, D. J. 1981. *J. Chem. Phys.* 74:4380–94
18. Balint-Kurti, G. G., Shapiro, M. 1981. *Chem. Phys.* 61:137–55
19. Shapiro, M., Bersohn, R. 1982. *Ann. Rev. Phys. Chem.* 33: 409–42
20. Starace, A. F. 1982. *Handb. Phys.* 31: In press
21. Berkowitz, J., Erhardt, H. 1966. *Phys. Lett.* 21:531–32
22. Niehaus, A., Ruf, M. W. 1972. *Z. Phys.* 252:84–94
23. Morgenstern, R., Niehaus, A., Ruf, M. W. 1970. *Chem. Phys. Lett.* 4:635–38
24. Dehmer, J. L., Chupka, W. A., Berkowitz, J., Jivery, W. T. 1975. *Phys. Rev. A* 12:1966–73
25. Carlson, T. A., Jonas, A. E. 1971. *J. Chem. Phys.* 55:4913–24
26. Karlsson, L., Mattson, L., Jadrny, R., Siegbahn, K., Thimm, K. 1976. *Phys. Lett. A* 58:381–84
27. Harrison, H. 1970. *J. Chem. Phys.* 52:901–5
28. Schönhense, G. 1981. *J. Phys. B* 14:L187–92
29. Flügge, S., Mehlhorn, W., Schmidt, V. 1972. *Phys. Rev. Lett.* 29:7–9
30. Oh, S. D., Pratt, R. H. 1974. *Phys. Rev. A* 10:1198–1203
31. Hall, J. L., Siegel, M. W. 1968. *J. Chem. Phys.* 48:943–45
32. Cooper, J., Zare, R. N. 1968. *J. Chem. Phys.* 48:942–43
33. Hotop, H., Lineberger, W. C. 1975. *J. Phys. Chem. Ref. Data* 4:539–76
34. Cooper, J., Zare, R. N. 1969. *Lectures in Theoretical Physics*, ed. S. Geltman, K. T. Mahanthappa, W. E. Brittin, 11-C:317–37. New York: Gordon & Breach
35. Tully, J. C., Berry, R. S., Dalton, B. J. 1968. *Phys. Rev.* 176:95–105
36. Buckingham, A. D., Orr, B. J., Sichel, J. M. 1970. *Philos. Trans. R. Soc. London Ser. A* 268:147–57
37. Peshkin, M. 1970. *Adv. Chem.Phys.* 18:1–14
38. Dehmer, J. L., Dill, D. 1979. *Electron Molecule and Photon Molecule Collisions*, ed. V. McKoy, T. Rescigno, B. Schneider, pp. 225–65. New York: Plenum

39. Dill, D. 1972. *Phys. Rev. A* 6:160–72
40. Raoult, M., Jungen, Ch., Dill, D. 1980. *J. Chim. Phys.* 77:599–604
41. Dehmer, J. L., Dill, D., Wallace, S. 1979. *Phys. Rev. Lett.* 43:1005–8
42. Stockbauer, R., Cole, B. E., Ederer, D. L., West, J. B., Parr, A. C., Dehmer, J. L. 1979. *Phys. Rev. Lett.* 43:757–61
43. West, J. B., Parr, A. C., Cole, B. E., Ederer, D. L., Stockbauer, R., Dehmer, J. L. 1980. *J. Phys. B* 13: L105–8
44. Cole, B. E., Ederer, D. L., Stockbauer, R., Codling, K., Parr, A. C., West, J. B., Poliakoff, E. D., Dehmer, J. L. 1980. *J. Chem. Phys.* 72:6308–10
45. Swanson, J. R., Dill, D., Dehmer, J. L. 1981. *J. Phys. B* 14:L207–11
46. Loge, G. W., Zare, R. N. 1981. *Mol. Phys.* 43:1419–28
47. Fano, U. 1957. *Rev. Mod. Phys.* 29:74–93
48. Fano, U., Racah, G. 1959. *Irreducible Tensorial Sets.* New York: Academic. 171 pp.
49. Brink, D. M., Satchler, G. R. 1968. *Angular Momentum.* Oxford: Clarendon. 160 pp. 2nd ed.
50. Blum, K. 1981. *Density Matrix Theory and Applications.* New York: Plenum. 217 pp.
51. Percival, I. C., Seaton, M. J. 1958. *Philos. Trans. R. Soc. London Ser. A* 251:113–38
52. Van Brunt, R. J., Zare, R. N. 1968. *J. Chem. Phys.* 48:4304–8
53. Case, D. A., McClelland, G. M., Herschbach, D. R. 1978. *Mol. Phys.* 35:541–73
54. Caldwell, C. D., Zare, R. N. 1977. *Phys. Rev. A* 16:255–62
55. Mauser, W., Mehlhorn, W. 1980. *Extended Abstracts of the 6th Int. Conf. Vacuum Ultraviolet Rad. Phys., Charlottesville, VA*, Vol. 2, Pap. 7, pp. 1–3
56. Klar, H. 1979. *J. Phys. B* 12:L409–12
57. Klar, H. 1980. *J. Phys. B* 13:2037–49
58. Theodosiou, C. E., Starace, A. F., Tambe, B. R., Manson, S. T. 1981. *Phys. Rev. A* 24:301–7
59. Greene, C. H., Zare, R. N. 1982. *Phys. Rev. A* 25: 2031–37
60. Grader, R. J., Oliver, A. J., Ebert, P. J. 1977. *Phys. Rev. A* 16:2388–91
61. Scofield, J. H. 1976. *Phys. Rev. A* 14:1418–20
62. Vigué, J., Grangier, P., Roger G., Aspect, A. 1981. *J. Phys. Paris* 42:L531–35
63. Rothe, E. W., Krause, U., Düren, R. 1980. *Chem. Phys. Lett.* 72:100–3
64. Chamberlain, G. A., Simons, J. P. 1975. *Chem. Phys. Lett.* 32:355–58
65. Chamberlain, G. A., Simons, J. P. 1975. *J. Chem. Soc. Faraday Trans. 2* 71:2043–50
66. Macpherson, M. T., Simons, J. P. 1977. *Chem. Phys. Lett.* 51:261–64
67. Macpherson, M. T., Simons, J. P. 1978. *J. Chem. Soc. Faraday Trans. 2* 74:1965–77
68. Macpherson, M. T., Simons, J. P. 1979. *J. Chem. Soc. Faraday Trans. 2* 75:1572–92
69. Poliakoff, E. D., Southworth, S. H., Shirley, D. A., Jackson, K. H., Zare, R. N. 1979. *Chem. Phys. Lett.* 65:407–9
70. Husain, J., Wiesenfeld, J. R., Zare, R. N. 1980. *J. Chem. Phys.* 72:2479–83
71. Loge, G. W., Wiesenfeld, J. R. 1981. *Chem. Phys. Lett.* 78:32–35
72. Poliakoff, E. D., Dehmer, J. L., Dill, D., Parr, A. C., Jackson, K. H., Zare, R. N. 1981. *Phys. Rev. Lett.* 46:907–10
73. Alder, K. 1952. *Helv. Phys. Acta* 25:235–58
74. Frauenfelder, H., Steffen, R. M. 1968. *Alpha-, Beta-, and Gamma-Ray Spectroscopy*, ed. K. Siegbahn, Vol. 2, Chap. 19A, pp. 997–1198. Amsterdam: North-Holland. 2nd ed.
75. Matthias, E., Olsen, B., Shirley, D. A., Templeton, J. E., Steffen, R. M. 1971. *Phys. Rev. A* 4:1626–58
76. Steffen, R. M., Alder, K. 1975. *The Electromagnetic Interaction in Nuclear Spectroscopy*, ed. Hamilton, pp. 505–643. Amsterdam: North Holland
77. Fano, U., Macek, J. H. 1973. *Rev. Mod. Phys.* 45:553–73
78. Fano, U., Dill, D. 1972. *Phys. Rev. A* 6:185–92
79. Dill, D., Fano, U. 1972. *Phys. Rev. Lett.* 29:1203–5
80. Dill, D. 1973. *Phys. Rev. A* 7:1976–87
81. Jackson, J. D. 1975. *Classical Electrodynamics*, p. 274. New York: Wiley. 848 pp. 2nd ed.
82. Blum, K. 1978. *Progress in Atomic Spectroscopy* ed. W. Hanle, H. Kleinpoppen, pp. 71–110. New York/London: Plenum
83. Macek, J., Hertel, I. V. 1974. *J. Phys. B* 7:2173–88
84. Hertel, I. V., Stoll, W. 1977. *Adv. At. Mol. Phys.* 13:113–228
85. Samson, J. A. R. 1969. *J. Opt. Soc. Am.* 59:356–57

86. King, G. C. M., Adams, A., Read, F. H. 1967. *J. Phys. B* 5:L254–57
87. Macek, J., Jaecks, D. H. 1971. *Phys. Rev. A* 4:2288–300
88. Blum, K., Kleinpoppen, H. 1979. *Phys. Rep.* 52:203–61
89. Hermann, H. W., Hertel, I. V. 1982. *Comments. At. Mol. Phys.* In press
90. Shurcliff, W. A. 1962. *Polarized Light: Production and Use*. Cambridge: Harvard Univ. Press. 207 pp.
91. Fano, U. 1949. *J. Opt. Soc. Am.* 39:859–63
92. Dill, D. 1976. *J. Chem. Phys.* 65:1130–33
93. Dill, D., Siegel, J., Dehmer, J. L. 1976. *J. Chem. Phys.* 65:3158–60
94. Davenport, J. W. 1976. *Phys. Rev. Lett.* 36:945–49
95. Smith, R. J., Anderson, J., Lapeyre, G. J. 1976. *Phys. Rev. Lett.* 37:1081–84
96. Ritchie, B. 1976. *Phys. Rev. A* 13:1411–15
97. Ritchie, B. 1976. *Phys. Rev. A* 14:359–62
98. Ritchie, B. 1976. *Phys. Rev. A* 14:1396–1401
99. Zare, R. N. 1971. *Acc. Chem. Res.* 4:361–67
100. Macek, J., Burns, D. 1976. *Topics in Current Physics*. Vol. 1: *Beam Foil Spectroscopy*, ed. S. Bashkin, pp. 237–64. New York: Springer-Verlag
101. Andrä, H. J. 1974. *Phys. Scr.* 9:257–80
102. Hafner, H., Kleinpoppen, H., Krüger, H. 1965. *Phys. Lett.* 18:270–71
103. Fano, U. 1957. *Nuovo Cimento* 5:1358–60
104. Fano, U. 1964. *Phys. Rev.* 135:B863–64
105. Alder, K., Winther, A. 1962. *Nucl. Phys.* 37:194–200
106. Greene, C. H. 1980. *Phys. Rev. Lett.* 44:869–71
107. Fano, U., Greene, C. H. 1980, *Phys. Rev. A* 22:1760–63
108. Zare, R. N., Herschbach, D. R. 1963. *Proc. IEEE* 51:178–82